Korean J. Chem. Eng., 34(2), 314-319 (2017)
DOI: 10.1007/s11814-016-0285-1

pISSN: 0256-1115
eISSN: 1975-7220

X-ray absorption spectroscopies of Mg-Al-Ni hydrotalcite like compound for explaining the generation of surface acid sites

Hong Khanh Dieu Nguyen*,†, Toan Dang Nguyen*, Dung Ngoc Hoang*, Duc Sy Dao, Thao Tien Nguyen**, Limphirat Wanwisa***, and Lan Linh Hoang****

*School of Chemical Engineering, Ha Noi University of Science and Technology, Ha Noi, Vietnam
**Faculty of Chemistry, Vietnam National University, Hanoi, Vietnam
***Synchrotron Light Research Institute (Public Organization), Nakhon Ratchasima, Thailand
****Vietnam National Oil and Gas Group, Vietnam
(*Received 25 July 2016 • accepted 11 October 2016*)

Abstract−Hydrotalcite-like compound containing metal cations such as Mg^{2+}, Al^{3+} and Ni^{2+} was characterized using Ni K-edge EXAFS and in situ Ni K-edge XANES techniques for clarifying its bonding environment around Ni^{2+} sites and structure changes during calcination from room temperature to 550 °C, respectively. At the fixed molar ratio of Mg/Ni/Al of 2/1/1, the results obtained from EXAFS analysis showed a slight blue shift before and after the calcination at 550 °C and a reduction in white line peak; the best fits of the two samples revealed tiny change in coordination number about 7 for Ni-O path but considerable difference for Ni-Mg(Al) path from about 4.5 to 9.5, confirming a modification from brucite like to mixed oxide structure. On the other hand, bond distances of the Ni-O and Ni-Mg paths nearly fixed at about 2.06 Å to 3.0 Å reflected stability of the cationic bond order on each plane, but partial collapse and decomposition of the interlayer formed by water molecules and anion CO_3^{2-} after the calcination. Linear combination fit extracted from the in situ Ni K-edge XANES also confirmed the changes along with the calcination such as slow and fast decreases of brucite fraction at 150 °C and 330 °C, respectively, in corresponding to the mixed oxide fraction increases. The achieved bonding structures were also applied to explain acid-base occurrence of the hydrotalcite-like material, especially the acid sites generated by different static charges along with the bonds. The explanation was illustrated by NH_3-TPD method.

Keywords: EXAFS, XAS, XANES, Hydrotalcite, Brucite

INTRODUCTION

Hydrotalcite is a natural mineral with general formula $Mg_6Al_2CO_3(OH)_{16}{\cdot}4(H_2O)$ formed by partial substitution of Al site (Al^{3+}) onto Mg site (Mg^{2+}) of brucite structure of $Mg(OH)_2$ [1,2]. Because of many unique and flexible properties, such as ordered crystalline structure, homogeneous cation distribution, strong base sites, "memory" effect and high surface area, hydrotalcite and hydrotalcite-like compounds play an important role in adsorption, ion exchange and catalysis applications [1,3-6]. Actually, for catalysis aspect, these materials have been used in many reactions such as polymerization of alkene oxides, aldol condensation, steam reforming of ethanol, hydrogenation reactions, oxidation reactions, support for Ziegler-Natta catalysts [1,7-11]. Recently, a series of hydrotalcite-like compounds have been used for vegetable oil decarboxylation processes or support for their hydrodeoxygenations to synthesize alternative green fuels, and their activity has been reported as potential catalysts or supports, being better and cheaper than commercial catalysts based on Co, Mo or Ni over alumina or carbon based materials [12-15]. Especially, introducing some metal cations into original hydrotalcite could considerably improve its catalytic properties. Gac [16] reported that when partially replacing of Mg^{2+} sites in the beginning hydrotalcite structure by Ni^{2+}, varying of molar Ni/Mg ratios strongly impacted acid-base property of the formed material, but the reason for that result remains unclearly. Casenave et al. [4] estimated acid-base properties of Mg-Ni-Al mixed oxides using hydrotalcite as precursor, and a relation between Ni content added to hydrotalcite and acid-base relation was also reported as introducing Ni leading to strengthen its acidity. The basicity reached a peak or the highest concentration when the content of Mg and Ni was low and high, respectively. They recommended a synergy effect of these metals favoring the basic properties and the role of MgO as promoter. However, the generation of acid sites was not fully understood. Tanabe's theory [17] also mentioned the generation and strengthening of base sites when incorporating of transition metal ions into MgO, but that of acid sites strongly depend on the bonding environment of the host and guest cations.

Recently, the XAS (X-ray absorption spectroscopy) including XANES (X-ray absorption near-edge structure) and EXAFS (Extended X-ray absorption fine structure) were used to explaining the generation of acidity in one of our materials - the meso-structured silica-calcium mixed oxide (MSCMO) catalyst [18], based on the different charges along the Ca-O-Si bonding system. The bonding environment of metal sites in the material could be well clari-

†To whom correspondence should be addressed.
E-mail: dieuhongprof@gmail.com

fied, confirming the powerful ability of the techniques.

Our purpose in this study focused on clarifying structure characteristics and explaining the generation of acid sites of Mg-Al-Ni hydrotalcite-like compound and mixed oxide system formed after its calcination using EXAFS and in situ XANES techniques. The bond environment around Ni site was deeply analyzed, providing a reliable aspect for simulating the structure of these materials, including coordination number, bond distance and bond energy around Ni sites. The acidity was also confirmed by NH_3-TPD method.

EXPERIMENTAL

1. Preparation of Mg-Ni-Al Hydrotalcite Like Compound

Mg-Ni-Al hydrotalcite material with Mg/Al/Ni molar ratio of 2/1/1 was prepared by co-precipitation method based on the work of Romero [9]. Mother solutions of Al(III), Ni(II) and Mg(II) nitrates (0.5; 0.5 and 1 mol/*l*, respectively) were prepared by dissolving $Al(NO_3)_3{\cdot}9H_2O$, $Ni(NO_3)_2{\cdot}6H_2O$ and $Mg(NO_3)_2{\cdot}6H_2O$ in distilled water, respectively. Material precursor was prepared by homogeneous precipitation method in carbonate alkaline solution, for which solutions containing Ni(II)-Mg(II)-Al(III) in given ratio were aged at 363 K during 24 h in PP bottle. The reaction was quenched by submitting the bottles into an ice-bath. The precipitate was centrifuged, washed with distilled water and dried at 373 K overnight followed by calcination at 550 °C for 6 hours in air flow. The materials before and after calcination at 550 °C were termed as HT3 and HT3-550.

2. Characterizations

In situ XANES measurements were done at beamline 2.2 Time-resolved XAS (TRXAS) of the Siam Photon Source, Thailand. The synchrotron was operated at 1.2 GeV with maximum ring current of 150 mA. XANES was measured in transmission mode at Ni K-edge. The XANES spectrum of the samples was taken at every 5 °C when the sample temperature was increased from room temperature to 550 °C. Static EXAFS spectra at Ni K-edge were measured for the as-prepared materials before and after calcination at beamline 8 XAS of Siam Photon Source. All EXAFS spectra were measured in transmission mode using double monochromator equipped with Ge 220. The energy of monochromator was calibrated with Ni foil at K-edge before the measurement. The samples were dilute with BN and put in sample holders whose windows were Kapton.

XANES spectra of in situ experiment were analyzed by using a linear combination fitting method. Under high temperature, the samples underwent structural and chemical changes. At the simplest level of analysis, we assumed that there existed only two species during the heating process. XANES at room temperature and that at 550 °C after 100 minutes were used as base spectra for initial and final products, respectively. All other spectra taken between room temperature and 500 °C were composed by the base spectra at certain fraction. The normalized XANES spectra were fitted using LCF tool of X-ray analysis software Athena. Energy fitting range was −20 eV to 30 eV, and no energy shift was included for the fit. This range covered most features of the XANES Ni K-edge.

EXAFS spectra at Ni K-edge were k^3 weighted and fitted in R space using Artemis, X-ray analysis software in the Ifeffit package. Fitting k range was 2.9-12.6 $Å^{-1}$ for all samples. Fourier transforms of these spectra were fitted from 1 Å - 3±0.05 Å. Initial hydrotalcite structure used for EXAFS refinement was derived from a well-established XRD structure [19]. In the XRD structure of Al^{3+} and Mg^{2+} were not distinguishable. Mg and Ni were included to the model structure by replacing Al ion. From the initial structure, the scattering amplitude and phase were calculated using the standard FEFF 9.6 program [20]. Single scattering paths Ni-O and Ni-X (X=Ni, Mg) were included for EXAFS refinement. All scattering paths shared the same fitting energy correction, E_0. The refinements were performed without background fit. To obtain the coordination number, the value of amplitude reduction S_0^2 was fixed for all samples. This value was extracted by fitting Ni K-edge EXAFS spectrum of Ni foil. In this fit, only Debye-Waller factors of single and multiple Ni-Ni scattering and path energy correction were fitted. The extracted value of S_0^2=0.84 was in good agreement with previously used value [21].

Powder XRD of the samples was recorded on a D8 Advance Bruker diffractometer using Cu Kα (λ=0.15406) radiation. NH_3-TPD method was measured on a Micromeritics Autocue II 2920 V4.01.

RESULTS AND DISCUSSIONS

1. Powder XRD

Stack powder XRD patterns of the HT3, HT3-550 and standard hydrotalcite [22] are plotted in Fig. 1. Positions of peaks characterizing for (003), (006), (101) (012)… were all detected in the XRD pattern of the sample HT3, illustrating a successive hydrotalcite-like compound preparation. However, the intensity/background ratio of the peaks in the HT3 was lower than that of the standard corresponding to the effect of the Ni^{2+} isomorphous substitution onto the position of Mg^{2+} [1]. The XRD pattern of the HT3-550 showed an interesting result relating to collapse of the crystalline structure when annealing the HT3 at 550 °C. This collapse indicated that the hydrotalcite-like structure of the sample HT3 was unstable under

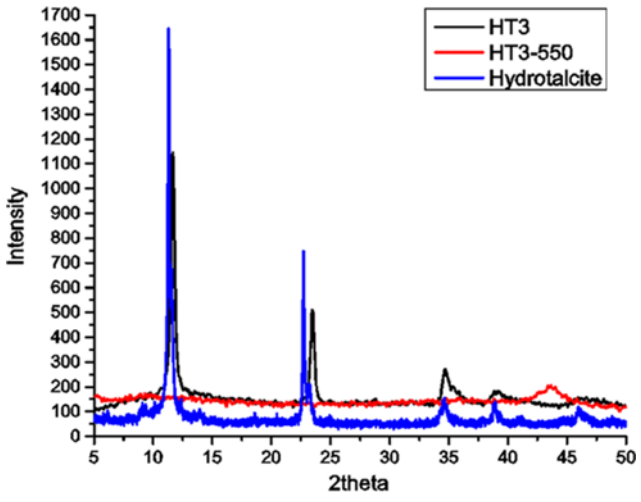

Fig. 1. XRD patterns of the HT3, HT3-550 and standard hydrotalcite.

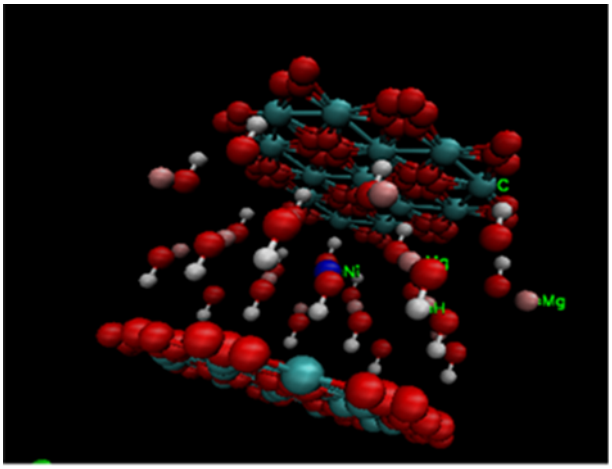

Blue: Ni, red: O, cyan: C, pink:

Fig. 2. The model structure for the EXAFS analysis.

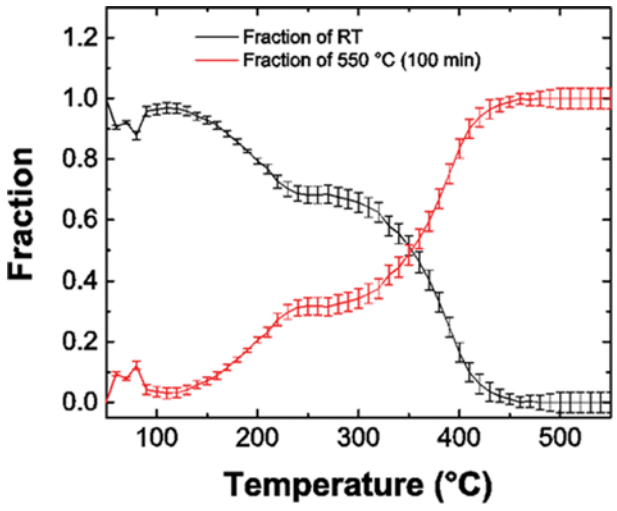

Fig. 4. Extracted fraction from LCF using room temperature and 550 °C, 100 minute as base spectra.

heat treatment. However, the collapse revealed a good agreement with some studies [23,24].

The results obtained from XRD pattern allowed us to build a structure simulation of the Mg-Ni-Al hydrotalcite-like compound (the sample HT3) in the same characteristics with standard hydrotalcite [22]. The only difference was the partial substitution of Ni^{2+} onto the position of Mg^{2+}. The model in Fig. 2 would be used in the EXAFS analysis thereafter.

2. In Situ Ni K-edge XANES of the Sample HT3 in Calcination Process

Fig. 3 shows selected XANES spectra of the sample HT3 when being heated from room temperature to 550 °C. As the temperature increased, the intensity of white line peak reduced; at the same time there was a trend of slight blue-shift ~1 eV from room temperature to 550 °C. The features ranging from 8,390 eV to 8,500 eV were not changed very much until 350 °C. This reflected as a plateau region in the fraction plot derived from LCF analysis (Fig. 4).

XANES at room temperature and 550 °C represented hydrotalcite-like structure and mixed oxide species, respectively. As shown in Fig. 4, a fraction of the hydrotalcite-like structure started to decrease slowly from 150 °C, which led to an increase in fraction of mixed oxides. The fractions stayed nearly flat from 220 °C to 330 °C. After this region of temperature population of the hydrotalcite-like structure quickly decreased, resulting in a quick increase in concentration of mixed oxides. These results were suitable to thermal analysis reported by [24]. In which, the region from room temperature to about 200 °C was assigned for water removal in both physical and structural forms; the region occurring at above 350 °C was described for thermal decomposition of interlayer anions CO_3^{2-}. As a consequence, when the interlayer decomposition took place, the hydrotalcite-like structure could collapse and transform to a mixed oxide system.

3. Ni K-edge EXAFS Analysis of the Samples HT3 (Before Calcination) and HT3-550 (After Calcination at 550 °C)

Fig. 5 shows normalized Ni K-edge XAS spectra of the HT3 and HT3-550 materials. As mentioned above, there was a blue shift about 1 eV from the HT3 to HT3-550 standing for changing from room temperature to 550 °C.

The radial structure function (RSF) resulting from Fourier transform of the k^3-weighted EXAFS in the range of 3-12.6 $Å^{-1}$ of the

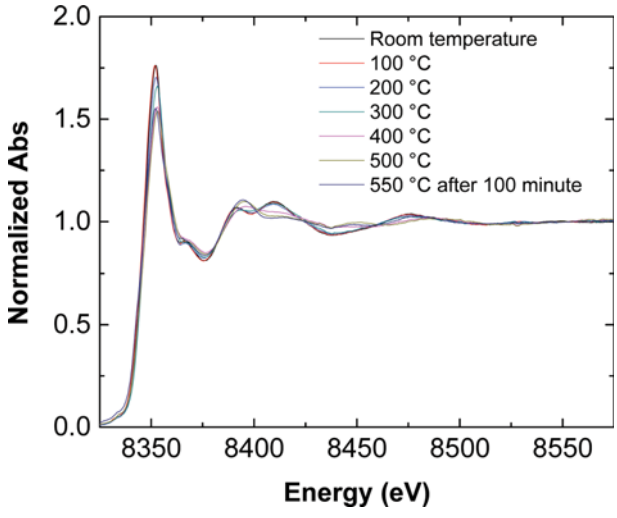

Fig. 3. XANES spectra of HT3 at different temperatures.

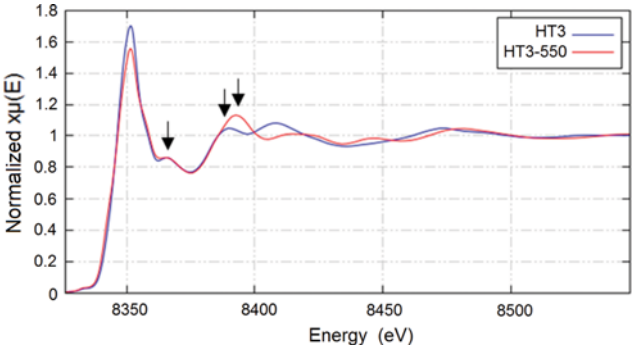

Fig. 5. XAS spectra of the samples HT3 and HT3-550.

HT3 and HT3-550 samples is shown in Fig. 4. The first peak centered ~1.6 Å resulted from Ni-O scattering. The second peak, which corresponded to second shell scattering, was contributed by Ni- X where X was either Ni or Mg. As can be seen, positions of the Ni-O peak were not changed as hydrotalcite was calcined in the HT3-550 material. However, the second peak, which was Ni-Mg, was shifted to smaller distance as hydrotalcite heated.

EXAFS refinements of the HT3 and HT3-550 were performed based on given model of the Mg-Ni-Al hydrotalcite like compound in Fig. 2, in which the Mg and Al sites were indistinguishable. Figs. 6 and 7 showed the k^3-weighted $\chi(k)$ plots for the two experimental data and their best fit, respectively. Overall, the structural model did an excellent job of fitting. A summary of the extracted parameters is presented in Table 1.

For these samples with Mg/Ni/Al molar ratio of 2/1/1, we found that Ni-Mg scattering was the main contribution of the second shell. This was verified when both Ni-Mg and Ni-Ni paths were included in EXAFS fitting of the second shell. The fit showed that Ni-Ni contribution was negligible. This was reasonable considering ratio

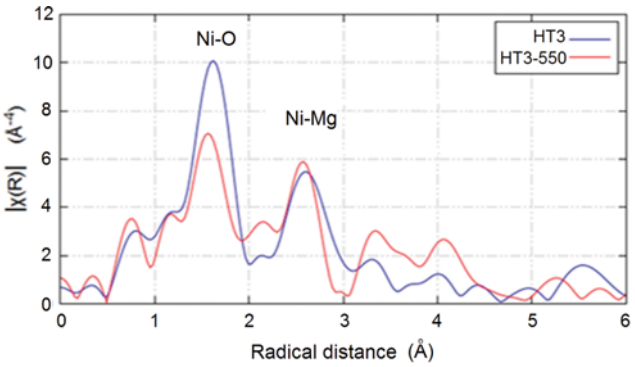

Fig. 6. Radial plot of HT3 and HT3-550. These plots were not phase corrected.

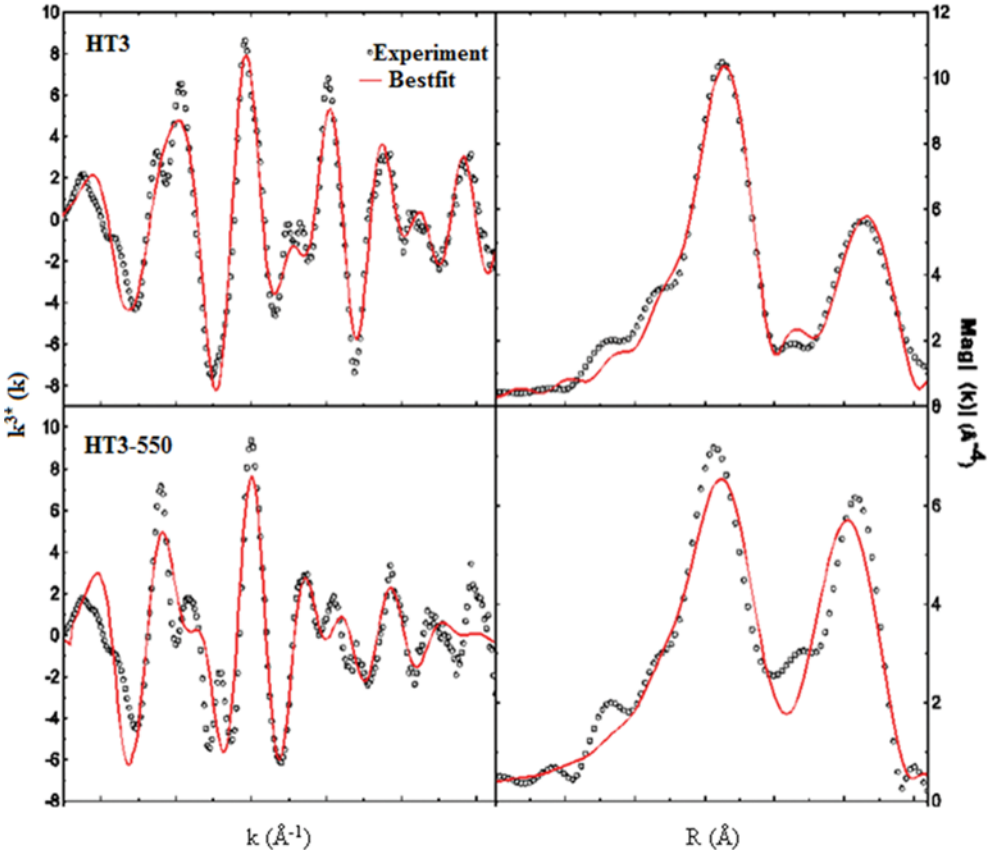

Fig. 7. EXAFS refinement for samples HT3 and HT3-550 plotted in k-space weighted by k^3 and plotted in R-space. Radial plots were not phase corrected.

Table 1. The best fit results obtained from EXAFS analysis of the HT3 and HT3-550

Samples	Scattering paths	N	R (Å)	σ^2 (Å^2)	ΔE (eV)	R factor
HT3	Ni-O	6.8(±0.6)	2.052(±0.007)	0.0068(±0.0009)	3.79(±1.03)	0.0075
	Ni-Mg	4.4(±0.8)	3.027(±0.007)	0.0033(±0.0014)		
HT3-550	Ni-O	7.0(±2.4)	2.075(±0.016)	0.0108(±0.0040)	5.51(±2.51)	0.0407
	Ni-Mg	9.5(±2.3)	2.937(±0.023)	0.0116(±0.0028)		

content of Mg and Ni in the samples.

The coordination numbers of Ni-O in the samples HT3 and HT3-550 nearly remained, indicating the first shell stability, but there were large differences with these values of Ni-Mg between the two samples. The difference indicated considerable changes in thermal treatment of the HT3 at 550 °C, and the second shell around Ni^{2+} sites was unstable, clearly caused by the collapse of the crystalline structure in heating process.

Bond distances of the Ni-O and Ni-Mg paths nearly fixed at about 2.06 Å to 3.0 Å for both the HT3 and HT3-550 samples, reflecting the stability of the cationic bond order on each plane in spite of collapse and partial decomposition of the interlayer formed by water molecules and anion CO_3^{2-} after the calcination.

4. Using the Results of the EXAFS Analysis for Explaining the Acid Generation of the Samples HT3 and HT3-500

A new hypothesis regarding the acidity generation of binary oxides proposed by Tanabe et al. [17,25] was applied in this study to explain acidic generation of the materials. In which, the hypothesis predicted what kinds of binary oxides would show acidic properties (Brønsted or Lewis acid) and provided insight regarding the structure of the acid sites. According to the hypothesis, acidity generation was caused by an excess of a negative or positive charge in the model structure of a binary oxide. The model structure was pictured according to the following two postulates: i) The coordination number of a positive element of a metal oxide, C1, and that of a second metal oxide, C2, were maintained even when mixed; ii) The coordination number of a negative element (oxygen) of a major component oxide was retained for all the oxygens in a binary oxide. Therefore, the bonding structure of the sample HT3 before calcination could be simulated as follows: Ni-O(6.8)-Mg(4.4). In which, the coordination number of oxygen was maintained at four because the Mg site dominates in the material. According to this simulation, two positive charges of Ni sites were distributed to 6.8 bonds of oxygen, while the two negative charges of the oxygen atom were distributed to six bonds. Hence, the difference in charge for one bond of the Ni and O sites was +2/6.8-2/4=−7/34, and for all 6.8 bonds was of −7/34×6.8=−1.4. In this case, Brønsted acidity was assumed to appear, because some protons were considered to associate with the oxygens to keep electric neutrality.

The bonding structure of the sample HT3-550 could also be described as Ni-O(7.0)-Mg(9.5), so the different charge along Ni-O bond was +2/7.0-2/4=−3/14, and for all 7 bonds around Ni sites was −3/14×7=−1.5 assigned for Brønsted acid sites on the sample surface. The different negative charges appeared along Ni-O bonds of the two samples reflecting a stronger acidity of the HT3-550 than that of the HT3.

The acidity of the two samples was also confirmed by NH_3-TPD method as described in Fig. 8. As the obtained results, both of the sample HT3 and HT3-550 possessed medium and strong acid sites with all the maximum desorption temperatures ranging from 200-400 °C and higher than 400 °C. From the maximum temperature aspect, the sample HT3-550 reached the highest peak at 544 °C when that of the sample HT3 was 457 °C, indicating the stronger acidity of the HT3-550 compared with the HT3. Although the STP NH_3 desorbed volume of the HT3 was higher than that of the HT3-550, the peak concentrations of the two samples were

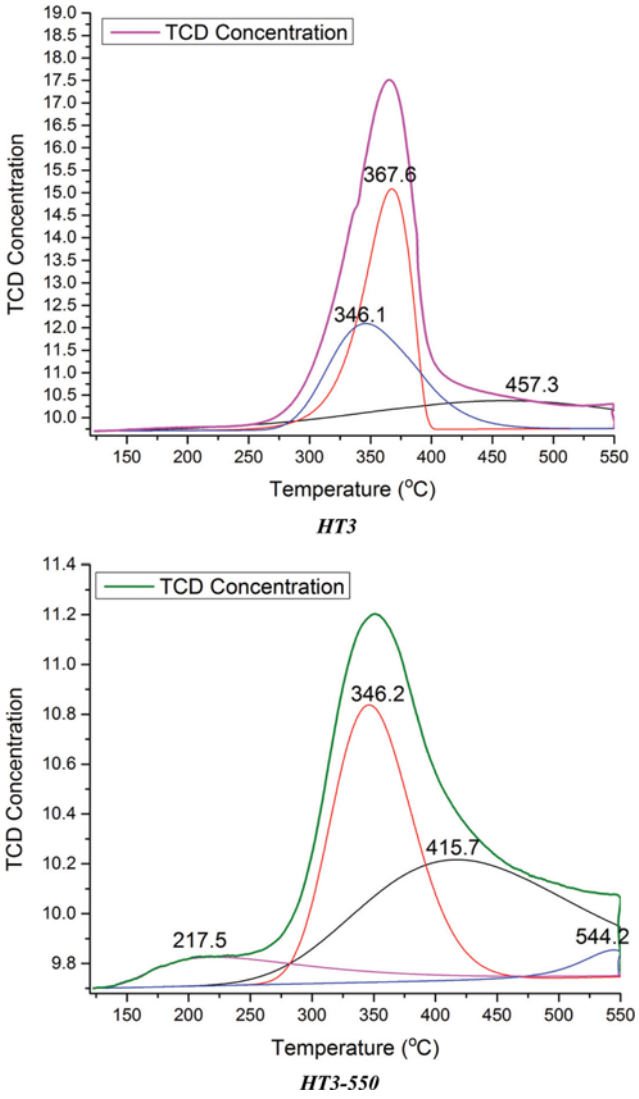

Fig. 8. NH_3-TPD diagrams and calculated parameters for maximum desorption temperatures, STP quantities of desorbed NH_3 and peak concentrations of each type of acidity. In which, strong, medium and weak acid sites correspond to maximum desorption temperatures of higher than 400 °C, range from 200 to 400 °C and less than 200 °C, respectively.

nearly equal. Therefore, the total acidity of the HT3-550 was higher than that of the HT3, confirming the obtained results from the combination of the EXAFS analysis and the Tanabe hypothesis.

CONCLUSION

The Mg-Ni-Al hydrotalcite-like compounds before and after calcination were characterized for thoroughly understanding their structure and bonding environment around Ni sites. The incorporation of Ni^{2+} onto Mg^{2+} positions remained beginning brucite-like layers, but this crystalline structure was unstable with thermal treatment followed by collapse into amorphous material. The stability of the coordination numbers and bond distances in the first shell around Ni^{2+} sites indicated the stability of the cationic bond-

ing order even when the crystalline layers collapsed. The phenomenon presented a transformation from hydrotalcite-like structure to mixed oxide system during calcination. The structure and coordination of Ni^{2+} sites generated acid sites on the material surface, and they also affected acid properties of the material before and after thermal treatment.

ACKNOWLEDGEMENT

This work was financially supported by the National Foundation for Science and Technology Development, Vietnam (NAFOSTED) under grant number 104.05-2013.57.

REFERRENCES

1. F. Cavani, F. Trifiro and A. Vaccari, *Catal. Today*, **11**, 173 (1991).
2. Q. Wang, H. Huang T., Z. Guo, L. Chen, Y. Liu, J. Chang, Z. Zhong, J. Luo and A. Borgna, *Appl. Clay Sci.*, **55**, 18 (1991).
3. S. Albertazzi, F. Basile and A. Vaccari, *Interface Sci. Technol.*, **1**, 496 (2004).
4. S. Casenave, H. Martinez, C. Guimon, A. Auroux, V. Hulea, A. Cordoneanu and E. Dumitriu, *Thermochim. Acta*, **379**, 85 (2001).
5. J. Yang and J. Kim, *Korean J. Chem. Eng.*, **23**(1), 77 (2006).
6. M. Khitous, Z. Salem and D. Halliche, *Korean J. Chem. Eng.*, **33**(2), 638 (2016).
7. O. Kikhtyanin, L. Hora and D. Kubicka, *Catal. Commun.*, **58**, 89 (2015).
8. A. Fonseca L., J. David A. B. and E. Moreira A., *Appl. Catal. A: Gen.*, **388**, 77 (2010).
9. A. Romero, M. Jobbagy, M. Laborde, G. Baronetti and N. Amadeo, *Appl. Catal. A: Gen.*, **470**, 398 (2014).
10. J. Yu, J. Li, H. Wei, J. Zheng, H. Su and X. Wang, *J. Mol. Catal. A: Chem.*, **395**, 128 (2014).
11. J. Zhang, S. Wu, Y. Liu and B. Li, *Catal. Commun.*, **35**, 23 (2013).
12. J. G. Na, B. E. Yi, J. N. Kim, K. B. Yi, S. Y. Park, J. H. Park, J. N. Kim and C. H. Ko, *Catal. Today*, **156**, 44 (2010).
13. J. G. Na, J. K. Han, Y. K. Oh, J. H. Park, T. S. Jung, S. S. Han, H. C. Yoon, S. H. Chung, J. N. Kim and C. H. Ko, *Catal. Today*, **185**, 313 (2012).
14. H. S. Roh, I. H. Eum, D. W. Jeong, B. E. Yi, J. G. Na and C. H. Ko, *Catal. Today*, **164**, 457 (2011).
15. H. K. D. Nguyen, V. V. Pham and H. T. Do, *Catal. Lett.*, **146** (2016), DOI:10.1007/s10562-016-1873-8.
16. W. Gac, *Appl. Surface Sci.*, **257**, 2875 (2011).
17. K. Tanabe, *Solid acids and bases: Their catalytic properties*, Kodansha Ltd. (1970).
18. H. K. D. Nguyen and T. D. Nguyen, *J. Porous Mater.* (2016), DOI: 10.1007/s10934-016-0279-8.
19. M. Bellotto, B. Rebours, O. Clause, J. Lynch, D. Bazin and E. Elkaim, *J. Phys. Chem.*, **100**, 8527 (1996).
20. J. Rehr, J. Kas, M. Prange, A. Sorini, Y. Takimoto and F. Vila, *Comptes Rendus Physique*, **10**, 548 (2009).
21. G. Sheng, S. Yang, J. Sheng, J. Hu, X. Tan and X. Wang, *Environ. Sci. Technol.*, **45**, 7718 (2011).
22. R. T. Downs, K. L. Bartelmehs and G. V. Gibbs, *American Mineralogist*, **78**, 1104 (1993).
23. C. Enrique D., J. Gallego, F. Mondragon, S Moreno and R. Molina, *Fuel*, **89**, 592 (2010).
24. L. Obalova, M. Valaskova, F. Kovanda, Z. Lacny and K. Kolinova, *Chem. Papers*, **58**, 33 (2004).
25. K. Tanabe, M. Misono, Y. Ono and H. Hattori, *Studies in Surface Science and Catalysis*, **51** (1989).